RSC Advances

ROYAL SOCIETY OF CHEMISTRY

www.rsc.org/advances

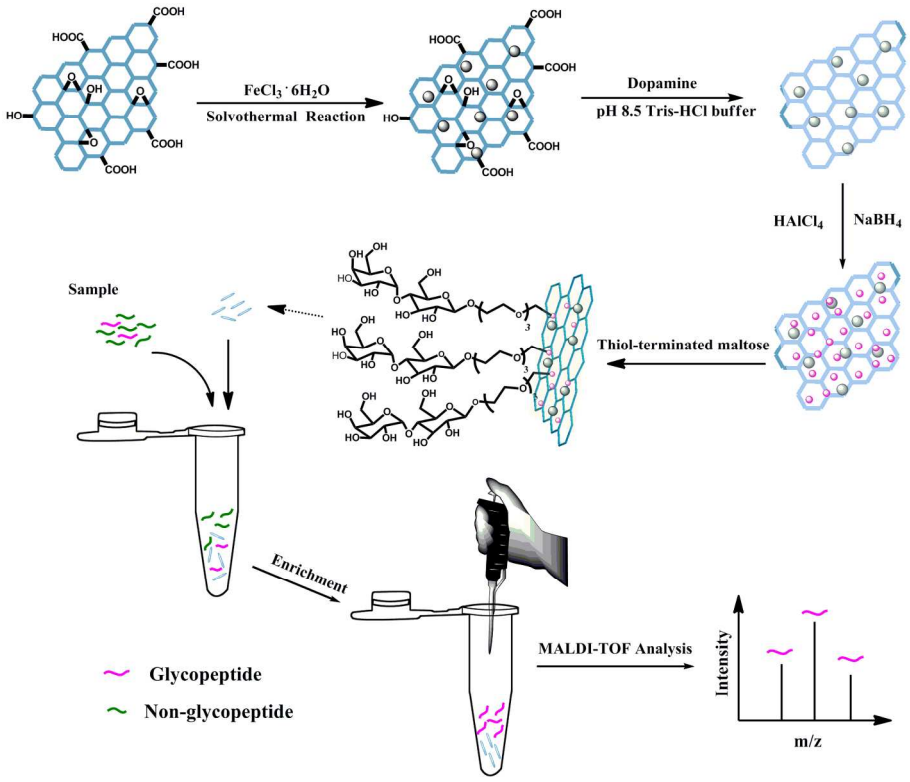

A novel and efficient approach was developed to synthesize hydrophilic thiol-terminated maltose-functionalized Au NPs/PDA/Fe_3O_4-RGO nanocomposite which exhibited high selectivity and detection sensitivity in the enrichment of glycopeptides from the complex samples.

Journal Name

ARTICLE

Synthesis of hydrophilic maltose functionalized Au NPs/PDA/Fe_3O_4-RGO magnetic nanocomposite for highly specific enrichment of glycopeptides

Received 00th January 20xx,
Accepted 00th January 20xx

DOI: 10.1039/x0xx00000x

www.rsc.org/

Changfen Bi,[a,b] Ruidong Jiang,[a,b] Xiwen He,[a,b] Langxing Chen[a,b,*] and Yukui Zhang[a,b,c]

The development of methods to isolate and enrich low-abundance glycopeptides is an important prerequisite for glycoproteomics research. In this study, a hydrophilic maltose functionalized Au nanoparticles (NPs)/polydopamine (PDA)/Fe_3O_4- reduced graphene oxide（RGO）nanocomposite has been successfully synthesized in mild conditions. The bioadhesive polydopamine film was prepared by self-polymerization on the surface Fe_3O_4-graphene oxide, which not only prevents the agglomeration graphene sheets and enhances the specific surface, but also facilitates the Au NPs immobilization. A great number of loading Au NPs possess the highly available surface area for the immobilization of the high density of thiol-terminated maltose via Au-S bond. The resulting Au NPs-maltose/PDA/Fe_3O_4-RGO nanocomposite exhibits excellent environmental stability, good biocompatibility and water dispersibility. Furthermore, the highly loaded Fe_3O_4 NPs makes the enrichment very convenient. With all of the advances, the novel Au NPs-maltose/PDA/Fe_3O_4-RGO nanocomposite presents selective enrichment of glycopeptides from the low concentration of horseradish peroxidase tryptic digest (0.1 ng μL^{-1}).

1. Introduction

As one of the most common post-translational modifications of proteins, glycosylations play important roles in physiological process, such as immune response, receptor-ligand interactions and signal transduction.[1,2] Anomalous glycosylations are considered to be correlated with numerous diseases, such as cancer,[3] neurodegenerative disorders[4] and other genetic abnormalities.[5,6] Thus, obtaining the information of glycopeptides is significant to understand glycoprotein functions in biological pathways and disease development as well as biomarker discovery.[7,8] Up to now, mass spectrometry (MS) has become an effective tool for analyzing glycopeptides/glycoproteins. However, direct analysis of low-abundance glycoproteins and glycopeptides extracted from the complex biological samples by MS is a great challenge, because the signals of low-abundance glycoproteins and glycopeptides are suppressed by billion-fold excess quantities of a few highly abundant proteins, making enrichment steps an important prerequisite for successful analysis.[9-11]

Over the past decade, several methods for isolation/enrichment of glycopeptides have been developed, including lectin affinity chromatography,[12,13] hydrazide chemistry,[14,15] boronic acid chemistry[16,17] and hydrophilic interaction chromatography (HILIC).[18,19] Among them, HILIC, which relies on the physical interactions between glycans and stationary, has aroused much interest due to its unbiased enrichment towards different glycopeptides, remarkable reproducibility and MS compatibility for separation of polar compounds. However, high selectivity gave a great challenge to glycopeptides enrichment. One of the most promising approaches to solve this issue is the development of novel HILIC materials. In recent years, maltose modified HILIC attracted more and more attention, due to superior selectivity and a narrow elution window than Sepharose, which can be explained by the flexible saccharide chain.[20,21] On the other hand, several HILIC stationary materials are prepared on the silica,[22,23] Sepharose[24] and magnetic nanoparticles,[25,26] but the aggregation of particles limits the available surface area of adsorbent for the efficient enrichment.

Graphene and its derivatives (such as graphene oxide, GO, and reduced graphene oxide, RGO) has attracted a great deal of attention in sample pretreatment due to its ultrahigh specific surface area, high loading capacity, large delocalized π-electron system and hydrophobic interaction.[27-29] However, how to achieve efficiently isolate the graphene and targets from the samples has some technological challenges, due to the easy stacking of graphene sheets and the relatively low density of surface functional groups. And many efforts have been devoted to overcome these challenges. Depositing nanoparticles on GO sheets can also prevent graphene

[a] Research Center for Analytical Sciences, College of Chemistry, Tianjin Key Laboratory of Biosensing and Molecular Recognition, State Key Laboratory of Medicinal Chemical Biology, Nankai University, Tianjin 300071, China
[b] Collaborative Innovation Center of Chemical Science and Engineering (Tianjin), Tianjin 300071, China
[c] Dalian Institute of Chemical Physics, Chinese Academy of Sciences, Dalian 116023, P. R. China. E-mail: ykzhang@dicp.ac.cn (Y. K. Zhang)

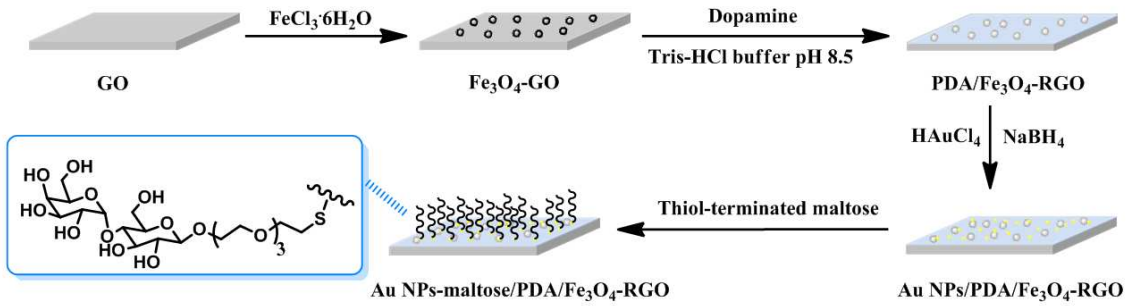

Scheme 1 Schematic illustration of the fabrication of hydrophilic magnetic Au NPs-maltose/PDA/Fe_3O_4-RGO nanocomposites.

nanosheets from restacking and thus endow new functionality to this 2D carbon nanomaterial.[30] As we know, iron oxide nanoparticles (Fe_3O_4 NPs) have the properties of good hydrophilicity, biocompatibility and magnetic responsibility[31-33] which will facilitate the separation process in comparison with conventional approaches. The hybrid of graphene and Fe_3O_4 NPs could effectively broaden the applicability[34]. On the other hand, dopamine commonly known as a neuroendocrine transmitter and a unique molecule mimicking the adhesive proteins, has been found to be able to polymerize into a unique hydrophilic polydopamine (PDA) coating on the organic and inorganic surface in mild condition.[35-38] Yang et al. reported that PDA as the adhesive coating on graphene sheets prevents the agglomeration graphene sheets and enhances the specific surface.[39] Meanwhile, The PDA coating remain stable even if in harsh environment such as strong acid solution, so it can protect the magnetic particles from etching in acid solution. Meanwhile, there are the strong adhesive forces and electrostatic interactions between PDA and gold NPs. As a result, gold NPs could be fabricated on the surface of the PDA.[40,41]

In this work, we report a facile approach to synthesize a novel hydrophilic magnetic composite Au NPs-maltose/PDA/Fe_3O_4-RGO. This nanocomposite has the following merits: (1) The large specific surface area of reduced graphene oxide (RGO) offers higher capacity for loading the Au NPs and thus possesses the highly available surface area for the immobilization of maltose. (2) The hydrophilic PDA layer on the magnetic graphene exhibits excellent environmental stability, good biocompatibility and good water dispersibility. (3) Lots of thiol-terminated maltose molecules were assembled onto Au NPs via Au-S bound, improving its hydrophility. Further, the long organic chains, bridging the Au NPs and thiol-terminated maltose could suppress the non-specific adsorption. (4) The highly loaded Fe_3O_4 NPs makes the enrichment very convenient. The resulting nanocomposite was successfully applied to highly selective capture glycopeptides from the complex biosamples.

2 Experimental

2.1 Materials

Horseradish peroxidase (HRP) (MW~ 44 kDa), bovine serum albumin (BSA), DL-Dithiothreitol (DTT), UREAand High Performance Liquid Chromatography (HPLC)-grade Acetonitrile (ACN) were purchased from Sigma-Aldrich (USA). Graphene oxide (GO) was obtained from XF NANO (China). 2, 5-dihydroxybenzoic acid (DHB), Iodoacetamide (IAA), dopamine hydrochloride and hydrogen tetrachloroaurate (ш) trihydrate ($HAuCl_4 \cdot 3H_2O$) were obtained from Alfa Aesar (USA). Amberlite IR120 was obtained from J&K (China). Urea, Iron(ш) chloride hexahydrate ($FeCl_3 \cdot 6H_2O$), anhydrous sodium acetate (NaAc), ethylene glycol (EG), sodium borohydride ($NaBH_4$), ammonium bicarbonate (NH_4HCO_3), formic acid (FA), D-maltose, acetic anhydride (Ac_2O), potassium thioglycolate (KSAc), sodium hydroxide (NaOH), paratoluensulfonyl chloride (TsCl), tetraethylene glycol, anhydrous sodium sulfate (Na_2SO_4), dichloromethane (CH_2Cl_2), methanol, ethanol, sodium, n-hexane, petroleum ether, ethyl acetate were purchased from Tianjin Chemical Reagent Company (Tianjin, China). Deionized water (18.25 MΩ cm) was prepared with a Milli-Q water purification system (Millipore, Milford, MA, USA).

2.2 Preparation of Fe_3O_4-GO nanocomposites

Fe_3O_4-GO nanocomposites were synthesized with a solvothermal method.[42] Typically, GO (48.7 mg), NaAc (1.36 g), $FeCl_3 \cdot H_2O$ (152 mg) were dissolved in EG (30 mL) under sonication to give a homogenous solution and then poured into a Teflon-lined stainless-steel autoclave (50 mL). After reaction at 180 °C for 16 h, the Fe_3O_4-GO nanocomposites were washed with deionized water and ethanol several times, then dried at 50 °C overnight.

2.3 Preparation of PDA-coated Fe_3O_4-GO Nanocomposites (PDA/Fe_3O_4-RGO)

The dopamine hydrochloride (30 mg) was added into a solution of Fe_3O_4-GO (40 mg) in 10 mM Tris buffer (pH 8.5). The reaction solution was sonicated for 10 min, and stirred vigorously at 60 °C for 24 h. The product of PDA/Fe_3O_4-RGO was washed with deionized water and ethanol thrice, then dried at 50 °C overnight.

2.4 Preparation of Au NPs/Fe_3O_4-RGO and Au NPs/PDA/Fe_3O_4-RGO nanocomposite

Into a solution of Fe_3O_4-RGO (or PDA/Fe_3O_4-RGO) nanocomposite (40 mg) in deionized water (60 mL) was added 24 mL

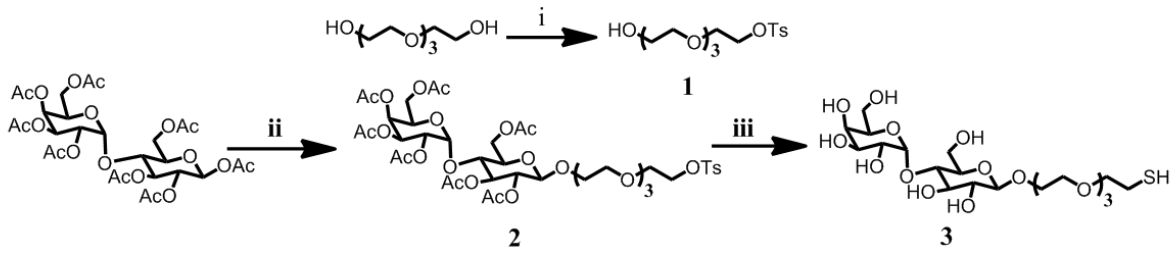

Scheme 2 Synthesis of the thiol-terminated maltose 3 Reagents and conditions: (i) TsCl, NaOH, THF, (0 °C);[45] (ii) $BF_3{\cdot}Et_2O$, CH_2Cl_2; (iii) a. KSAc, 2-butanone, b. 1M NaOMe/MeOH,MeOH.[46,47]

$HAuCl_4{\cdot}3H_2O$ (1 mg·mL^{-1}). The solution was sonicated for 5 min, and stirred for 2 h at room temperature. Then freshly prepared $NaBH_4$ (10 mg mL^{-1}) was added and stirred continuously for another 2 h. [43] The Au NPs/Fe_3O_4-RGO or Au NPs/PDA/Fe_3O_4-RGO nancomposites were washed with deionized water and ethanol thrice, then dried at 50 °C for 3 h.

2.5 Preparation of thiol-terminated maltose (3)

Reagents and condition for the preparation of thiol-terminated maltose (**3**) was shown in Scheme 2. The synthesis procedure of compounds **1-3** is in the following.

2-(2-(2-(2Hydroxyethoxy)ethoxy)ethoxy)ethyl p-tosylate (**1**)

Into a solution of tetraethylene glycol (21.95 g, 113 mmol) in CH_2Cl_2 (4 mL) was added an aqueous NaOH (0.69 g, 17.13 mmol) solution (4 mL) dropwise at 0 °C under nitrogen atmosphere, and then a THF solution (20 mL) of p-toluenesulfonyl chloride (2.08 g, 10.93 mmol) was added dropwise slowly. The resulting mixture was allowed to stir at 0 °C for 2 h. The reaction mixture was poured into ice H_2O (70 mL), and the solvent was concentrated to ~2/3 volume under reduce pressure. The remaining solution was extracted with CH_2Cl_2 (3 × 60 mL), and the combined organic layers were washed with brine (40 mL), and dried over Na_2SO_4. The crude mixture was filtered, concentrated and purified by silica gel chromatography (ethyl acetate / petroleum ether, 30:70 to 70:30) to give the product as a pale yellow oil (5.53 g, 20.4 %).

2-(2-{2-[2-(2-Tosyloxy-ethoxy)-ethoxy]-ethoxy}-ethyl) 2,3,4,6-tetra-O-β-D-glucopyranosyl-(1→4)-2,3,6 tri-O-acetyl-β-D-glucopyranoside (**2**)

Into a solution of cta-O-acteyl-D-maltopyranose (3.72 g, 5.5 mmol) and 1 (1.58 g, 6.0mmol) was added $BF_3{\cdot}Et_2O$ (2.4 mL, 8.4 mmol) at 0°C under a nitrogen atmosphere. After stirring 24h at room temperature, the reaction mixture was diluted with $NaHCO_3$, extracted with CH_2Cl_2, washed with brine, and then dried over Na_2SO_4. After filtration of the crude mixture, the crude product was concentrated and purified by silica gel chromatography (ethyl acetate/hexane 50:50~ 80:20) to give the product as a pale yellow oil (1.38 g, 26 %).

2-(2-{2-[2-(2-thiol-ethoxy)-ethoxy]-ethoxy}-ethyl)-β-D-glucopyranosyl -(1→4)- β-D-glucopyranoside (**3**)

Into a solution of 2 (1.5 g, 1.55 mmol) in 2-butanone (30 mL) was added potassium thioacetate (0.35 g, 3.1 mmol). The resulting mixture was stirred under refluxing for 2 h. The solvent were evaporated under reduced pressure, then the residue was dissolved with CH_2Cl_2 (100 mL) and washed with brine. The organic layer was dried over Na_2SO_4 and evaporated under reduced pressure. After purified by silica gel chromatography (ethyl acetate/petroleum ether 30:30~ 50:50), the residue was solved into dry MeOH, and added NaOMe/MeOH (0.84 M, 1 eq) at 0 °C under nitrogen atmosphere. The resulting mixture was stirred at room temperature for 3h. The reaction mixture was neutralized by Amberlite IR 120 H until pH 6, after filtration the solvent was evaporated under reduced pressure to give the product as a pale brown oil. ^{1}H NMR(400 M Hz, DMSO, δ, ppm): 5.53~ 5.48(m, 2H), 5.14(d, J= 4.8 Hz, 1 H), 5.00 (d, J = 3.7 Hz, 1 H), 4.94 (m, 2 H), 4.54 (m, 2 H), 4.20 (d, J = 7.7 Hz, 1 H), 3.89 ~ 3.85 (m, 1 H), 3.72 ~ 3.42 (m, 19 H), 3.35~ 3.16 (m, 4 H), 3.09 ~ 3.00 (m, 2 H), 2.90 (t, J = 6.4 Hz, 1 H), 2.61 (t, J = 6.68 Hz, 1 H), 2.51 ~ 2.50 (m, 1H). HR MS (ESI): Calcd for $C_{20}H_{38}O_{14}S$ [M+ Na]$^+$ 557.1874, found 557.1876.

2.6 Preparation of Au NPs-maltose/Fe_3O_4-RGO and Au NPs-maltose/PDA/Fe_3O_4-RGO nanocomposite

Into a solution of Au NPs/Fe_3O_4-RGO or Au NPs/PDA/Fe_3O_4-RGO nanocomposite (30 mg) in ethanol (60 mL) was added thiol-terminated maltose (300 mg). The solution was sonicated for 5 min, and stirred at room temperature for 24 h[44]. With a magnetic separation technique, the Au NPs/Fe_3O_4-RGO or Au NPs-maltose/PDA/Fe_3O_4-RGO composite was washed with ethanol thrice, then dried at 50 °C for 3 h.

2.7 Characterization

The morphology and structure of the synthesized magnetic graphene composites were evaluated using a Tecnai G2T2 S-TWIN transmission electron microscope (TEM). Samples for TEM were prepared by placing a drop of dilute particles of solution in the ethanol solvent on a copper grid. The infrared spectra were recorded on a Nicolet AVATAR-360 Fourier transform infrared (FT-IR) spectrometer. After vacuum drying, the samples were thoroughly mixed with KBr (the weight ratio of sample/KBr was 1%) in a mortar, and then the fine powder was pressed into a pellet. The identification of the crystalline phase was performed on a Rigaku D/max/2500v/pc (Japan) X-ray diffractometer with a Cu Ka source. The 2θ angles probed were from 3° to 80° at a rate of 4°min^{-1}. The hydrophilicity were evaluated with contact angle analyzer JCY-1 (Fangrui,

China). The magnetic properties were analyzed with a vibrating sample magnetometer (VSM) (LDJ 9600-1, USA).

2.8 Enrichment of glycopeptides

The tryptic digest of HRP was prepared in the following. Typically, HRP was dissolved in NH_4HCO_3 (50 mM, pH 8.0) to the final concentration (1 mg·mL^{-1}) and denatured at 100 °C for 5 min. Then, trypsin was added into the solution at an enzyme/substrate ratio of 1: 50 (w/w) and incubated at 37 °C for 16 h. The digestion of BSA was performed by incubating a mixture of 1mg BSA, 100 μL 8 M urea and 20 μL in 50 mM NH_4HCO_3 solution (pH 8.0) at 56 °C for 1 h, and then mixing 20 μL 200mM IAA at 37 °C in the dark for 30 min, then adding 860 μL NH_4HCO_3 solution and trypsin in the mixture at enzyme/ protein ratio of 1:50 (w/w) for 12 h at 37 °C. After the addition of formic acid (5 μL) to quench the reaction, the tryptic digestion was stored at -20°C until use.

Au NPs-maltose/PDA/Fe_3O_4-RGO nanocomposites (1 mg) were added into HRP digests or mixed sample (HRP, BSA digests) (400 μL) dissolved in CH_3CN/H_2O/FA (80: 19.9: 0.1) with shaking for 1 h at RT, it was then washed thrice with the same solution (CH_3CN/H_2O/FA= 88: 19.9: 0.1, 3× 400 μL, 10 min) to remove the nonspecifically adsorbed peptides. A solution of CH_3CN/H_2O/FA (10: 89: 1, 15 μL) was added to release the glycopeptides at RT for 30 min. The elutes were analyzed by MALDI-TOF MS.

2.9 MALDI-TOF MS analysis

MALDI-TOF MS analysis was performed on a Autoflex III LRF 200- CID TOF/TOF mass spectrometer (Bruker Daltonics, Bermen, Germany). The DHB matrix was prepared by adding 2, 5-dihydroxybenzonic acid (DHB, 12 mg) into a solution of CH_3CN/H_2O/FA (30:69:1). Equivalent amounts (1 μL) of elute and DHB matrix were sequentially dropped onto the MALDI plate for MS analysis. The MALDI mass spectra were obtained in positive-ion reflector mode.

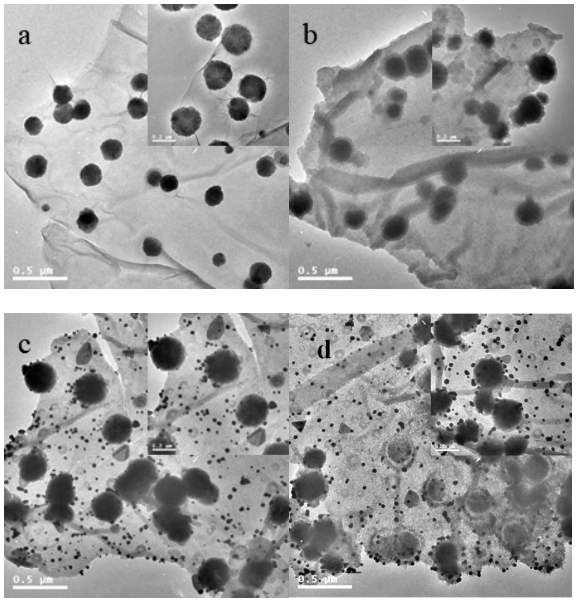

Figure 1 TEM images of Fe_3O_4-GO (a); PDA/Fe_3O_4-RGO (b); Au NPs/PDA/ Fe_3O_4-RGO (c); Au NPs-maltose/PDA/Fe_3O_4-RGO (d) nanocomposites.

3 Results and discussion

3.1 Preparation and Characterization of Au NPs-maltose/PDA/ Fe_3O_4-RGO nanocomposites

The stepwise fabrication of Au NPs-maltose/PDA/Fe_3O_4-RGO nanocomposites is illustrated in Scheme 1. Firstly, magnetic graphene oxide (Fe_3O_4-GO) was synthesized with a solvothermal method.[42] The GO highly loaded with Fe_3O_4 NPs is hydrothermally produced from the reduction reaction between $FeCl_3$ and ethylene glycol in the presence of GO. Secondly, dopamine was oxidized to form PDA layer on the surface the Fe_3O_4-GO. The step is vital, because PDA layer not only protects the stability of magnetic nanoparticles and improves the hydrophilicity of graphene, but also maintains the good dispersion of gold nanoparticles (Au NPs) on the surface of RGO for further functionalization. Thirdly, Au NPs were loaded on the surface of PDA through the sodium borohydride reduction. Finally, the highly dense thiol-terminated maltose **3** was assembled onto the surface of Au NPs with Au-S bond to form Au NPs-maltose/PDA/Fe_3O_4-RGO nanocomposites.

The sizes and morphology of the products of Fe_3O_4-GO, PDA/Fe_3O_4-RGO, Au NPs/PDA/Fe_3O_4-RGO and Au NPs-maltose/PDA/Fe_3O_4-RGO nancomposites were characterized by TEM. As shown in Figure 1a, there are a lot of Fe_3O_4 NPs having an average diameter of approximate 200 nm which dispersed on the surface of the GO nanosheets. After formation of PDA coating by self-polymerization, the morphology of PDA/Fe_3O_4-RGO remains the inherent Fe_3O_4-GO sheets with the relative thick coating (Figure 1b). It can be seen from Figure 1c, there is a great amount of Au NPs with an average diameter of ~5 nm obviously loaded on the surface of PDA/Fe_3O_4-RGO sheets by direct reduction of $HAuCl_4$ using sodium borohydride as reducing agent. Meanwhile, Au NPs-maltose/PDA/Fe_3O_4-RGO nanocomposites indicated that the

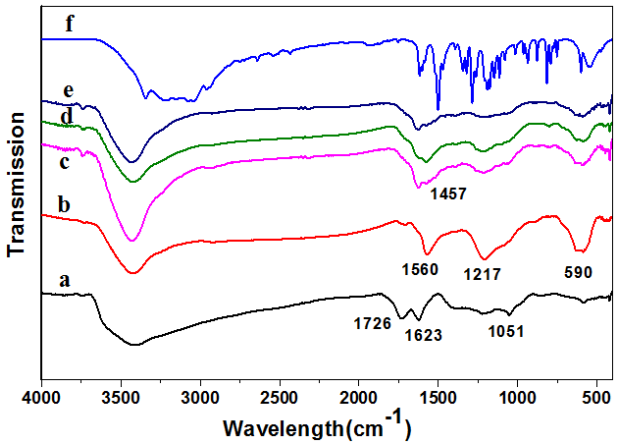

Figure 2 FT- IR spectra of GO (a), Fe_3O_4-GO (b), PDA/Fe_3O_4-RGO (c), Au NPs/PDA/Fe_3O_4-RGO (d), Au NPs-maltose/PDA/Fe_3O_4-RGO (e) nanocomposites and dopamine (f).

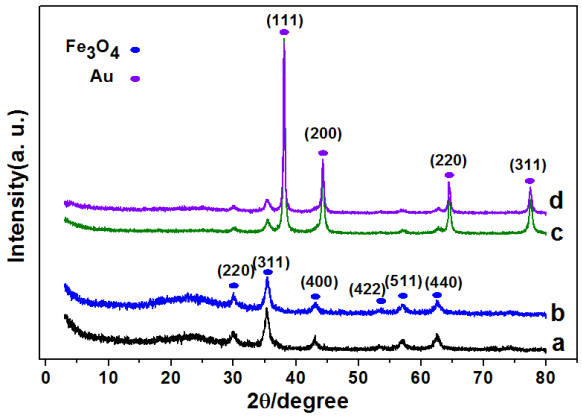

Figure 3 XRD patterns of Fe_3O_4-GO (a), PDA/Fe_3O_4-RGO (b) and Au NPs /PDA/Fe_3O_4-RGO (c) and Au NPs-maltose/PDA/Fe_3O_4-RGO nanocomposites.

modification of thiol-terminated maltose didn't cause agglomeration. (Figure 1d).

Fourier transform infrared (FT-IR) spectra in the range of 4000~ 450 cm^{-1} were employed to monitor the stepwise synthesis of Au NPs-maltose/PDA/Fe_3O_4-RGO nanocomposites. As shown in Figure 2a, the peaks at 1726 cm^{-1}, 1217 cm^{-1} and 1051 cm^{-1} were ascribed to the stretching vibration of C=O bond, C-O and C-O-C bond of the epoxy structures and -COOH in GO, respectively, while the band of 1623 cm^{-1} is assigned to C=C stretching vibration of graphene. The peaks of Fe_3O_4-GO (Figure 2b) at 590 cm^{-1} and 1560 cm^{-1} were assigned to the vibration Fe-O bond and anti-symmetrical vibration of COO^-. After coating the dopamine, the weak peak of PDA/Fe_3O_4-RGO (Figure 2c) at 1457 cm^{-1} was substituted by C-C vibration of the benzene ring. Compared to Fe_3O_4-GO, the C= O peak at 1720 cm^{-1} disappeared. It indicated that Fe_3O_4-GO was reduced to PDA/Fe_3O_4-RGO by the modification of PDA. Meanwhile, the characteristic peaks of Figure 2c/d/e were virtually identical, which demonstrated that the framework of PDA/Fe_3O_4-RGO remains unchanged.

The crystalline property of Fe_3O_4-GO, PDA/Fe_3O_4-RGO, Au NPs/PDA/Fe_3O_4-RGO and Au NPs-maltose/PDA/Fe_3O_4-RGO nanocomposite was characteriazed by X-ray diffraction (XRD). As shown in Figure 3, in the 2θ range of 3~80°, the characteristic peaks for Fe_3O_4 (2θ=30.1°, 35.5°, 43.1°, 53.4°, 57.1°, 62.7°) at the corresponding 2θ values are indexed as (220), (311), (400), (422), (511) and (440), respectively, which can be indexed to the face center-cubic phase of Fe_3O_4 (JCPDS Card no. 19- 629). Meanwhile, the diffraction peaks at 38.1°, 44.3°, 64.6°, 77.4° of Au NPs-maltose/PDA/Fe_3O_4-GO are observed, which represent the Bragg reflections from (111), (200), (220) and (311) planes of Au (JCPDS Card No. 01– 1174), showing clearly the existence of Au NPs in the Au NPs/PDA/Fe_3O_4-RGO and Au NPs-maltose/PDA/Fe_3O_4-RGO composites (Figure 3c, 3b). The magnetic properties of the synthesized nanocomposites were studied using a vibrating sample magnetometer (VSM) at room temperature. As shown in Figure 4, the magnetization saturation (*Ms*) values of Fe_3O_4-GO, PDA/Fe_3O_4-RGO, Au NPs/PDA/Fe_3O_4-RGO and Au NPs-maltose/PDA/Fe_3O_4-RGO nanocomposites were 40.09, 21.73, 16.69, 16.35 emu·g^{-1}, respectively. The decrease in *Ms* of PDA/Fe_3O_4-RGO in comparison

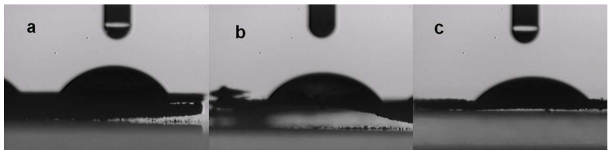

Figure 5 Shape of water drops on Fe_3O_4-GO (a), PDA/Fe_3O_4-RGO and Au NPs-maltose/PDA/Fe_3O_4-RGO nanocomposites.

with Fe_3O_4-GO is attributed to the increased mass of self-assembled polydopamine layer on the surface of Fe_3O_4-GO. The *Ms* value of Au NPs/PDA/Fe_3O_4-RGO was lower than PDA/Fe_3O_4-RGO, due to the modification Au NPs on the surface of PDA/Fe_3O_4-RGO. Nevertheless, after thiol-terminated maltose was functionalized on the surface of Au NPs, the *Ms* of Au NPs- maltose/PDA/Fe_3O_4-RGO remained about the same. And the magnetization value was sufficient to accomplish fast and efficient separation with an external

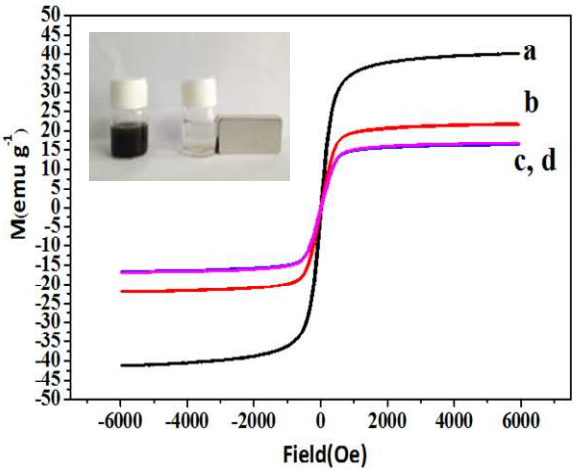

Figure 4 Hysteresis loops of magnetic Fe_3O_4-GO (a), PDA/Fe_3O_4-RGO (b), Au NPs/PDA/Fe_3O_4-RGO (c) and Au NPs-maltose PDA / Fe_3O_4-RGO (d) nanocomposites.

magnetic field. The resulting nanocomposite materials also show a fast response to the applied magnetic field (2000 Oe). After dispersing the Au NPs-maltose/PDA/Fe_3O_4-RGO in water by shaking, sonication, they can be easily separated within 30s with the help of the magnetic field (Figure 3 inset). This suggests that the novel nanocomposite materials possess excellent magnetic and redispersibility, which is advantageous to application in bioseparation.

To demonstrate the influence of the hydrophilicity of the nanocomposites on the enrichment, we have added the contact angle measurements for the composite materials in each step. Deionized water was used as a probe liquid. When deionized water was put on the membrane surface, the water contact angle was measured immediately average at three points. Generally, the smaller contact angle indicates the better hydrophilicity of materials. The contact angle of Fe_3O_4-GO (Figure 5a), PDA/Fe_3O_4-RGO (Figure 5b) and Au NPs-maltose/PDA/Fe_3O_4-RGO (Figure 5c) nanocomposites were 52.95°, 50.92° and 44.31° separately, implying the enhancement in in hydrophilicity after modified PDA and maltose.

3.2 Selective enrichment of glycopeptides

The selective isolation and enrichment of glycopeptides were based on the hydrophilic interaction between the hydrophilic maltose molecules and glycopeptides. To demonstrate the enhanced enrichment of glycopeptides due to the hydrophilicity of PDA and assembly of maltose on the surface of Au NPs, Fe_3O_4-GO, Au NPs-maltose/Fe_3O_4-RGO, Au NPs/PDA/Fe_3O_4-RGO and Au NPs-maltose/PDA/Fe_3O_4-RGO nanocomposites were used to enrich glycopeptides from HRP digests, respectively (Figure 6). The direct analysis of HRP digest (10 ng·μL^{-1}) without enrichment, only one peak (H7) could be observed, due to the suppression of non-glycopeptides (Figure 6A). The Fe_3O_4-GO without modification of hydrophilic PDA and maltose showed no enrichment (Figure 6B1). If the Au nanoparticles are immobilized on Fe_3O_4-GO directly and followed by hydrophilic maltose functionalization, there is no glycopeptides signals were detected (Figure 6B2). After the modification of polydopamine on graphene oxide with reference supporting, two glycosylated peptides were assigned without assembly of maltose (Figure 6C). Thankfully, after enrichment with Au NPs-maltose/PDA/Fe_3O_4-GO nanocomposites, non-glycosylated signals were removed effectively and the additional 8 glycosylated peptides could be identified except for peak H7. Moreover, the signal-to-noise (S/N) ratio of the glycopeptides was obviously enhanced (Figure 6D). The detailed structure of glycopeptides in

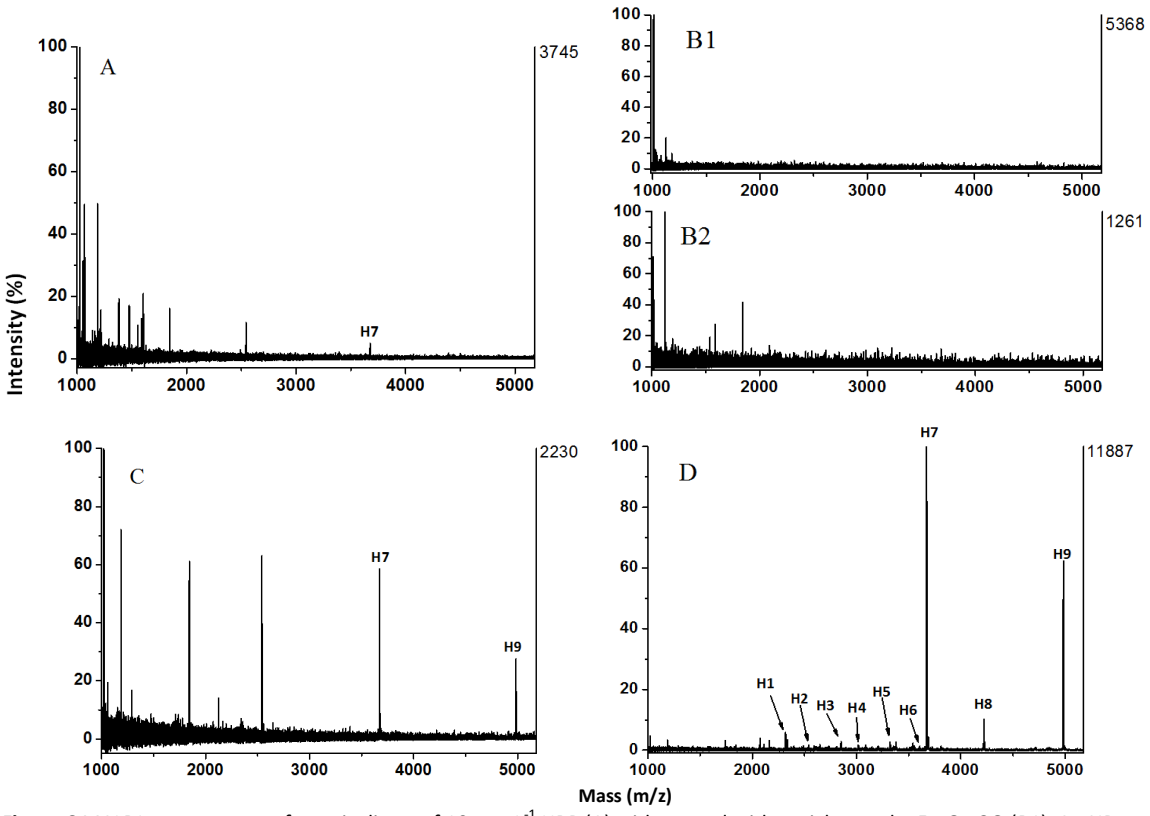

Figure 6 MALDI mass spectra of tryptic digest of 10 ng·μL^{-1} HRP (A) without and with enrichment by Fe_3O_4-GO (B1), Au NPs-maltose/Fe_3O_4-RGO (B2), Au NPs/PDA/Fe_3O_4-RGO (C) and Au NPs-maltose/PDA/Fe_3O_4-RGO (D) nanocomposites. The peaks of glycopeptides fragments are marked with H.

Table 1 Detailed information of the glycopeptides enriched by Au NPs-maltose/PDA/Fe_3O_4-RGO nanocomposites from HRP digests.[10]

Peak number	Observed m/z	Glycan composition	Amino acid sequence[a]
H1	2321.0	$Man_2GlcNAc_2$	MGN#ITPLTGTQGQIR
H2	2591.0	$XylMan_3FucGlcNAc_2$	PTLN#TTYLQTLR
H3	2850.0	FucGlcNAc	GLIQSDQELFSSPN#ATDTIPLVR
H4	3087.8	$XylMan_3FucGlcNAc_2$	GLCPLNGN#LSALVDFDLR
H5	3323.6	$XylMan_3FucGlcNAc_2$	QLTPTFYDNSCPN#VSNIVR
H6	3606.3	$XylMan_3FucGlcNAc_2$	NQCRGLCPLNGN#LSALVDFDLR
H7	3671.9	$XylMan_3FucGlcNAc_2$	GLIQSDQELFSSPN#ATDTIPLVR
H8	4223.3	$XylMan_3FucGlcNAc_2$	QLTPTFYDNSC(AAVESACPR)PN#VSNIVR
H9	4983.8	$XylMan_3FucGlcNAc_2$	LYN#FSNTGLPDPTLN#TTYLQTLR
		$XylMan_3FucGlcNAc_2$	

[a] The N-glycosylation sites are marked with N#. GlcNAc = N-acetylglucosamine, Fuc = fructose, Man = mannose, Xyl = xylose.

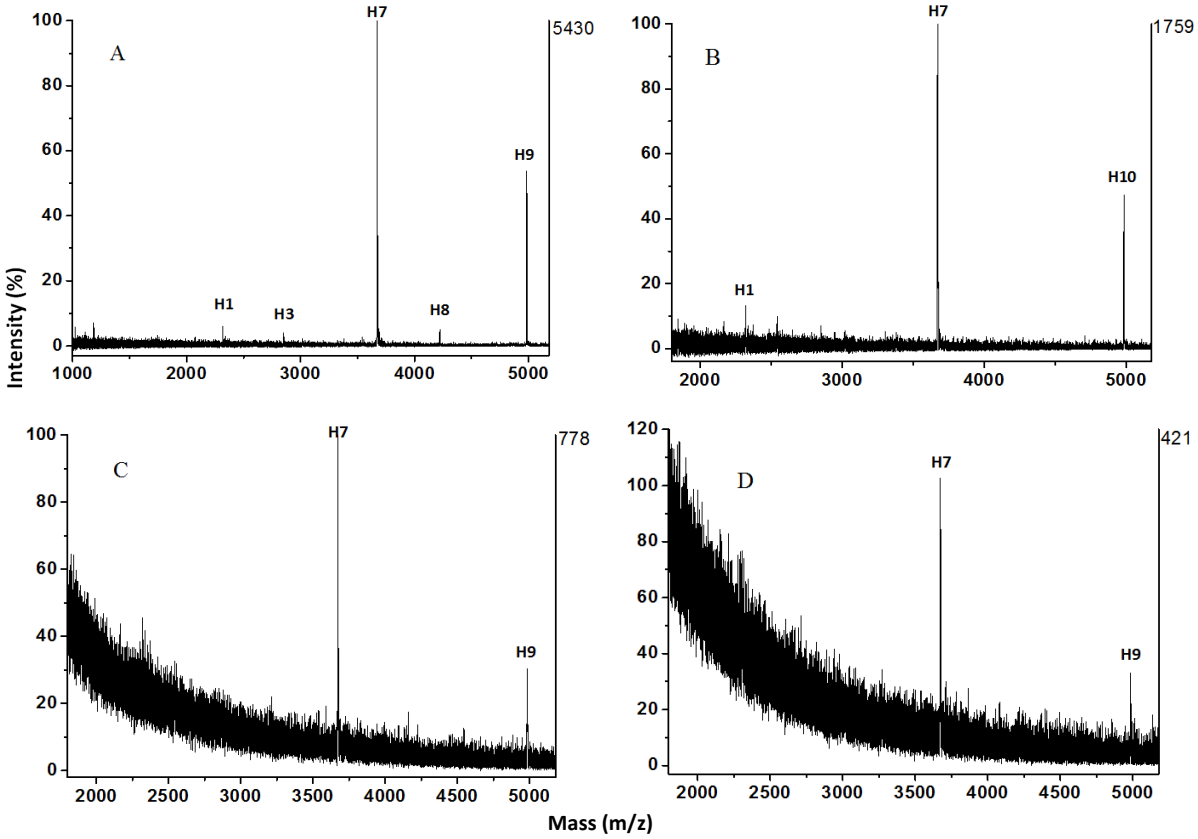

Figure 7 MALDI mass spectra of tryptic digest of (A) 5, (B) 1, (C) 0.2, (D) 0.1 ng·μL^{-1} HRP after enrichment with Au NPs-maltose/PDA/ Fe_3O_4-RGO nanocomposites.

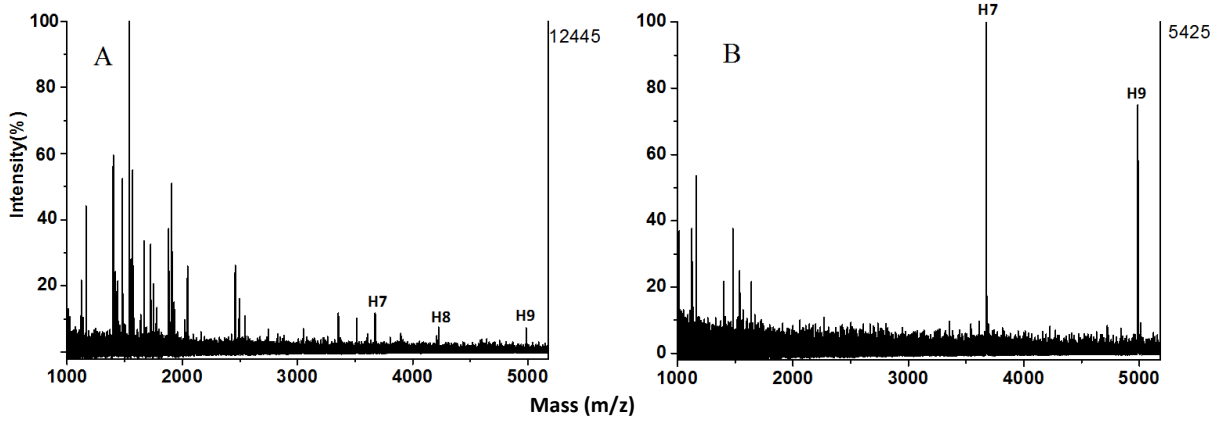

Figure 8 MALDI mass spectra of the tryptic digest mixture of HRP and BSA (1:10, mass ratio) (A) without and with enrichment by Fe_3O_4-GO Au NPs-maltose/PDA/ Fe_3O_4-RGO nanocomposites (B).

Figure 6D is listed in Table 1. The results indicate that the modification of PDA layer and maltose on the nanocomposite synergically contributed to improve its hydrophilicity which enhanced the selectivity of glycopepetides enrichment.

The sensitivity of the above prepared nanocomposites for glycopeptides was detected with different concentrations of the HRP tryptic digest. As shown in Figure 7, the glycopeptides peaks H1-H9 detected in the elutes of 10 ng·μL^{-1} HRP digests didn't appear except peaks H7 and H9 along with the decrease of the concentration of HRP digest. Nevertheless, there are two glycopeptide peaks (H7, H9) could be still observed after enrichment with Au NPs-maltose /PDA/Fe_3O_4-RGO nanocomposites from HPR digests (0.1 ng·μL^{-1}). The results indicate that hydrophilic Au NPs-maltose/PDA/Fe_3O_4-RGO nanocomposites can specifically extract glycopeptides from the HRP digest solution with high sensitivity.

The performance of composite material for glycopeptide enrichment from complicated peptide mixture or biological samples should be carried out. Figure 8A shows the direct analysis of the tryptic digest mixture of HRP and BSA (1:10, mass ratio), glycosylated peptides signal were suppressed absolutely. In contrast, after enrichment by Au NPs-maltose/PDA/Fe_3O_4-RGO nanocomposites (Figure 8B), 2 peaks (H7, H9) could be clearly detected. The results indicated that Au NPs-maltose/PDA/Fe_3O_4-RGO nanocomposites had high enrichment efficiency and selectivity for the glycopeptides from a complicated biosample.

Conclusions

In conclusion, a novel hydrophilic thiol-terminated maltose-functionalized Au NPs/PDA/Fe_3O_4-RGO nanocomposite was synthesized in mild conditions. Due to enhanced hydrophilic by PDA layer and suppressed nonspecific adsorption of non-glycosylated peptides by the organic chains bridging Au NPs and maltose, the resulting nanocomposite exhibited high selectivity and detection sensitivity in the enrichment of glycopeptides from the complex samples without any pretreatment. The novel nanocomposites are expected to become a promising strategy to design an efficient and sensitive tool for glycoproteomic analysis.

Acknowledgements

We gratefully appreciate the financial support by the National Basic Research Program of China (No. 2012CB910601), the National Natural Science Foundation of China (No 21275080, 21475067) and the Research Fund for the Doctoral Program of Higher Education of China (No. 20120031110007) and the National Natural Science Foundation of Tianjin (No. 15JCYBJC20600).

Notes and references

1 A. Helenius and M. Aebi, *Science*, 2001, **291**, 2361.
2 G. A. Rabinovich and M. A. Toscano, *Nat. Rev. Immuno.*, 2009, **6**, 338.
3 T. I. Williams, D. A. Saggese and D. C. Muddiman, *J. Proteome Res.*, 2008, **7**, 2562.
4 H. Hwang, J. P. Zhang, K. A. Chung, J. B. Leverenz, C. P. Zabetian, E. R. Peskind, J. Jankovic, Z. Su, A. M. Hancock, C. Pan, T. J. Montine, S. Pan, J. Nutt, R. Albin, M. Gearing, R. P. Beyer, M. Shi and J. Zhang, *Mass Spectrom. Rev.*, 2010, **29**, 79.
5 T. Hennet, Biochim. Biophys. Acta, 2012, 1820, 1306.
6 H. H. Freeze, E. A. Eklund, B. G. Ng and M. C. Patterson, *Lancet Neurol.*, 2012, **11**, 453.
7 S. J. Yang and H. Zhang, *Anal. Chem.*, 2012, **84**, 2232.
8 Z. C. Xiong, H. Q. Qin, H. Wan, G. Huang, Z. Zhang, J. Dong, L. Y. Zhang, W. B. Zhang and H. F. Zou, *Chem. Commun.*, 2013, **49**, 9284.
9 Y. Li, X. M. Zhang, C. H. Deng, *Chem. Soc. Rev.*, 2013, **42**, 8517.
10 R. N. Ma, J. J. Hu, Z. W. Cai and H. X. Ju, *Nanoscale*, 2014, **6**, 3150.
11 J. A. Ferreira, A. L. Daniel-da-Silva, R. M. P. Alves, D. Duarte, I. Vieira, L. L. Santos, R. Vitorino and F. Amado, *Anal. Chem.*, 2011, **83**, 7035.
12 K. Kubota, Y. Sato, Y. Suzuki, N. G. Inoue, T. Toda, M. Suzuki, S. I. Hisanaga, A. Suzuki and T. Endo, *Anal. Chem.*, 2008, **80**, 3693.
13 H Kaji, Y. Yamauchi, N. Takahashi and Isobe, *Nat. Protoc.*, 2006, **1**, 3091.
14 G. Huang, Z. Sun, H.Q. Qin, L. Zhao, Z. C. Xiong, X. J. Peng, J. J. Ou and H. F. Zou, *Analyst*, 2014, **139**, 2199.
15 T. Nishikaze, S. Kawabata, S. Iwamoto and K. Tanaka, *Analyst*, 2013, **138**, 7224.
16 Y. Y. Qu, J. X. Liu, K. G. Yang, Z. Liang, L. H. Zhang and Y. K. Zhang, *Chem. Eur. J.*, 2012, **18**, 9056.
17 Y. W. Xu, Z. X. Wu, L. J. Zhang, H. J. Lu, P. Y. Yang, P. A. Webley and D. Y. Zhao, *Anal. Chem.*, 2009, **81**, 503.
18 S. Mysling, G. Palmisano, P. Højurp and M. T. Andersen, *Anal. Chem.*, 2010, **82**, 5598.
19 Y. Shu, J. C. Lang, Z. S. Breitach, H. X. Qiu, J. P. Smuts, M. K. Shimobe, M. Yasuda and D. W. Armstrong, *J. Chromatogr. A.*, 2015, **1390**, 50.
20 J. Li, X. L. Li, Z. M. Guo, L. Yu, L. J. Zou and X. M. Liang, *Analyst*, 2011, **136**, 4075.
21 L. Yu, X. L. Li, Z. M. Guo, X. L. Zhang and X. M. Liang, *Chem. Eur. J.*, 2009, **15**, 12618.
22 A. J. Shen, Z. M. Guo, X. M. Cai, X. Y. Xue and X. M. Liang, *J. Chromatogr. A*, 2012, **1228**, 175.
23 P. Pomach, K. B. Chandler, R. Lan, N. Edwards, R. Goldman, *J. Proteome Res.*, 2012, **11**, 1728
24 L. Yu, X. L. Li, Z. M. Guo, X. L. Zhang and X. M. Liang, *Chem. Eur. J.*, 2009, **15**, 12618.
25 Z. C. Xiong, L. Zhao, F. J. Wang, J. Zhu, H. Q. Qin, R. A. Wu, W. B. Zhang and H. F. Zou, *Chem. Commun.*, 2012, **48**, 8138.
26 W. F. Ma, L. L. Li, Y. Zhang, Q. An, L. J. You, J. M. Li, Y. T. Zhang, S. Xu, M. Yu, J. Guo, H. J. Lu and C. C. Wang, *J. Mater. Chem.*, 2012, **22**, 23981.
27 A. K. Geim and K. S. Novoselov, *Nature Mater.*, 2007, **6**, 183.
28 S. T. Wang, M. Y. Wang, X. Su, B. F. Yuan and Y. Q. Feng, *Anal. Chem.*, 2012, **84**, 7763.
29 Y. Y. Zeng, H. J. Chen, K. J. Shiau, S. U. Hung, Y. S. Wang and C. C. Wu, *Proteomics*, 2012, **12**, 280.
30 X. F. Han, L. Zhang and C. Z. Li, *RSC Adv.*, 2014, **4**, 30536.
31 M. Mazur, A. Barras, V. Kuncser, A. Galatanu, V. Zaitzeu, K. V. Turcheniuk, P. Woisel, J. Lyskawa, W. Laure, A. Sirwardena, R. Boukherroub and S. Szunerits, *Nanoscale*, 2013, **5**, 2692.
32 H. W. Gu, K. M. Xu, C. J. Xu and B. Xu, *Chem. Commun.*, 2006, 941.
33 X. H. Zhang, X. W. He, L. X. Chen and Y. K. Zhang, *J. Mater. Chem.*, 2012, **22**, 16520.
34 G. Cheng, Y. L Liu, Z. G. Wang, J. L. Zhang, D. H. Sun and J. Z. Ni, *J. Mater. Chem.*, 2012, **22**, 21998.
35 Y. H. Yan, Z. F. Zheng C. H. Deng, Y. Li, X. M. Zhang and P. Y. Yang, *Anal. Chem.*, 2013, **85**, 8483.
36 J. H. Waite and M. L. Tanzer, *Science*, 1981, **212**, 1038.
37 L. Q. Xu, W. J. Yang, K.-G. Neoh, E.-T. Kang and G. D. Fu, *Macromolecules*, 2010, **43**, 8336.
38 C.-C. Ho and S.-J. Ding, *J. Mater. Chem. B*, 2015, **3**, 2698.
39 L. P. Yang, J. H. Kong, W. A. Yee, W. S. Liu, S. L. Phua, C. L. Toh, S. Huang and X. H. Lu, *Nanoscale*, 2012, **4**, 4968.
40 A. J. Ma, Y. X. Xie, J. Xu, H. B. Zeng and H. L. Xu, *Chem. Commun.*, 2015, **51**, 1469.
41 M. Zhang, X. W. He, L. X. Chen and Y. K. Zhang, *J. Mater. Chem.*, 2010, **20**, 10696.
42 Y. L. Liang, X. W. He, L. X. Chen and Y. K. Zhang, *RSC Advances*, 2014, **4**, 18132.
43 J. Tian, S. Y. Deng, D. L. Li, D. Shan, W. He, X. J. Zhang and Y. Shi, *Biosens. Bioelectron.*, 2013, **49**, 466.

44 X. L. Zhao, Y. Q. Cai, T. Wang, Y. L. Shi and G. B. Liang, *Anal. Chem.*, 2008, **80**, 9091.
45 V. Percec, P. Leomanawat, H. J. Sun, O, Kulikov, C. D. Nusbaum, T. M. Tran, A. Bertin, D. A. Wilson, M. Peterca, S. D. Zhang, N. P. Kamat, K. Moock, E. D. Johnston, D. A. hammer, D. J. Pochan, Y. C. Chen, Y. M. Chabre, T. C. Shiao, M. B. Brlek, S. André, R. Roy, H. J. Gabius and P. A. Heiney, *J. Am. Chem. Soc.*, 2013, **135**, 9055
46 K. D. Park, R. H. Liu and H. Kohn, *Chemistry& Biology*, 2009, **6**, 763.
47 C. L. Schofield, B. Mukhopadhyay, S. M. Hardy, M. B. McDonnell, R. A. Field and D. A. Russell, *Analyst*, 2008, **133**, 626.